

Thermally driven topology in frustrated systems

Jie-Xiang Yu,^{*} Morgan Daly, and Jiadong Zang

Department of Physics and Materials Science Program, University of New Hampshire, Durham, New Hampshire 03824, USA

 (Received 14 September 2018; revised manuscript received 9 January 2019; published 27 March 2019)

Topological spin textures, such as magnetic skyrmions, have been extensively discussed in magnetic materials with broken inversion symmetry. Most of these textures are stable at low temperatures and form long-range orders. However, the topological nature of these textures, characterized by the index called topological charge, is actually persistent at elevated temperatures. In this work, the topological charge of a two-dimensional frustrated spin model with the Dzyaloshinskii-Moriya (DM) interaction was calculated by the Monte Carlo simulations. At finite temperatures, nontrivial topology driven by thermal fluctuation was discovered in a spin-disordered phase. This thermally driven topology is the dominant topology at low magnetic fields. The magnitude of topological charge is quadratic in the DM interaction and linear in the external magnetic field or uniaxial magnetic anisotropy. We also propose a real frustrated system, the Mn-Bi monolayer film, with large DM interaction to enable such thermally driven topology. A full phase diagram of this system has been explored.

DOI: [10.1103/PhysRevB.99.104431](https://doi.org/10.1103/PhysRevB.99.104431)

I. INTRODUCTION

Low-dimensional magnetic systems have attracted long-term interest due to numerous exotic phenomena therein. Their recent marriage to topology has stimulated the development of the skyrmion physics. A magnetic skyrmion is a two-dimensional (2D) topological spin texture first discovered in B20 chiral magnets [1–6] in terms of small-angle neutron scattering and Lorentz transmission electron microscopy [1,2,7]. Although skyrmions have been extensively observed and discussed in many three-dimensional samples, mathematically speaking, the concept of a skyrmion is strictly defined in two dimensions. Each skyrmion has one-to-one correspondence to a unit sphere. Topology of the configuration itself has induced novel properties in the skyrmion dynamics and electronic/magnonic transports.

The topology of the skyrmion can be mathematically described in terms of the topological index dubbed the topological charge Q_T [8–10], which measures the coverage of a spin configuration on a unit sphere. In a smooth spin configuration respecting the continuum limit, Q_T can be written in the widely adopted form $Q_T = \frac{1}{4\pi} \int d^2r \mathbf{S} \cdot (\partial_x \mathbf{S} \times \partial_y \mathbf{S})$. However, once the spin configuration is rapidly changing, Q_T defined on the lattice should be used instead. To this end, one needs to triangulate the lattice and calculate the solid angle Ω expanded by three spins, \mathbf{S}_1 , \mathbf{S}_2 , and \mathbf{S}_3 , sitting on each vertex of each triangle. Q_T is related to Ω by $Q_T = \frac{1}{4\pi} \sum \Omega$, and Ω can be computed by the Berg formula [8]

$$e^{i\Omega/2} = \rho^{-1} [1 + \mathbf{S}_1 \cdot \mathbf{S}_2 + \mathbf{S}_2 \cdot \mathbf{S}_3 + \mathbf{S}_3 \cdot \mathbf{S}_1 + i\mathbf{S}_1(\mathbf{S}_2 \times \mathbf{S}_3)], \quad (1)$$

where $\rho = \sqrt{2(1 + \mathbf{S}_1 \cdot \mathbf{S}_2)(1 + \mathbf{S}_2 \cdot \mathbf{S}_3)(1 + \mathbf{S}_3 \cdot \mathbf{S}_1)}$ is a normalization factor and Ω ranges between -2π and 2π . In systems with periodic boundary conditions, the manifold is compact, and Q_T is always an integer number. As a simple example, the solid angle is zero everywhere for a ferromagnetic state, so that $Q_T = 0$. In contrast, a skyrmion covers a complete unit sphere, and the total solid angle is $\pm 4\pi$ depending on chirality, so that $Q_T = \pm 1$.

Skyrmions are well modeled in 2D chiral magnets, in which broken inversion symmetry induces the Dzyaloshinskii-Moriya (DM) [11] interaction [12]. In a finite window of the B - T phase diagram, the skyrmion crystal phase can be figured out. It is not surprising to have nonzero topological charge in this phase. However, as reported by our recent work, nonzero topological charge exists in a much wider range in the phase diagram [13]. Particularly, at large magnetic field, the topological charge is nonzero at finite temperatures and peaks around the melting temperature of the ferromagnetic state. Such emergence of the topological charge is actually driven by thermal fluctuations. In this regime, the spin configuration is completely random, and the topological charge spreads out over the whole lattice. The symmetry consideration suggests that the topological charge is linear in the external magnetic field B and quadratic in the DM interaction D . This thermally driven topology can be detected by the electric or thermal Hall effect [14–18]. Therefore, the correspondence between the skyrmion and topological charge is not one to one. The skyrmion definitely leads to nonzero topological charge, but nonzero topological charge does not necessarily indicate the presence of skyrmions. Nonzero topological charge should exist in a variety of 2D spin models, as long as the DM interaction is present.

The lattice under investigation is the simple hexagonal lattice, which can be regarded as a 2D hexagonal boron nitride structure with buckling, shown in Fig. 1. Two sublattices, labeled A and B , are located in two different atomic monolayers (MLs). Sublattice A is magnetic, and sublattice B is

^{*}Present address: Department of Physics, Center for Molecular Magnetic Quantum Materials and Quantum Theory Project, University of Florida, Gainesville, Florida 32611, USA; jiexiang.yu@unh.edu

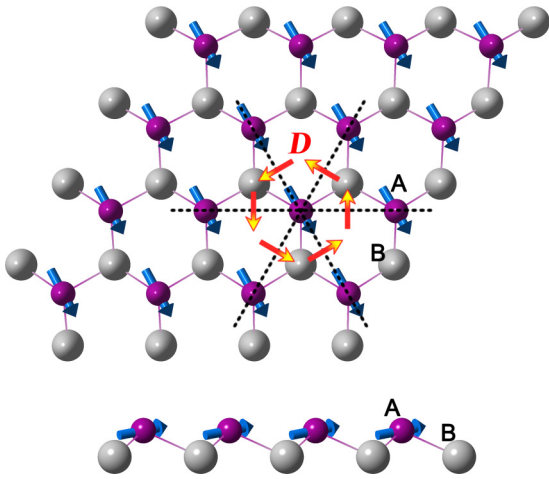


FIG. 1. Top view and side view of the crystal structure of a 2D hexagonal lattice with A - B sublattices. Only A sites have local magnetic moments. Three dashed lines give six nearest neighbors for each A site. Directions of the DM interactions \mathbf{D}_{ij} are sketched by six arrows.

heavy atoms such as $4d$ or $5d$ transition metal atoms with strong spin-orbit coupling (SOC). B sites are thus responsible for the DM interactions. This system has the point group C_{3v} without inversion symmetry, and it is also a prototype of many noncentrosymmetric magnetic film systems such as Fe/Ir(111) and Fe/Re(0001) [19–21]. Its Hamiltonian is given by

$$\mathcal{H} = \sum_{(i,j)} [J\mathbf{S}_i \cdot \mathbf{S}_j + \mathbf{D}_{ij} \cdot (\mathbf{S}_i \times \mathbf{S}_j)] - \sum_i \left[\frac{1}{2} K_u S_{iz}^2 + B S_{iz} \right], \quad (2)$$

where S_i and S_j are the two nearest-neighbor local magnetic moments at sites i and j of sublattice A . Each site has six nearest neighbors. The Heisenberg interaction J originates from the superexchange along the A - B - A path and direct exchange between neighboring A sites. The direction $\hat{\mathbf{D}}_{ij}$ of DM interaction $\mathbf{D}_{ij} = D \cdot \hat{\mathbf{D}}_{ij}$ is perpendicular to the bond connecting sites i and j according to the Moriya rule [12], as shown in Fig. 1. The second term in Eq. (2) includes on-site uniaxial magnetic anisotropy K_u and the Zeeman coupling with an external magnetic field B along the \hat{z} direction.

Antiferromagnetic coupling, namely, $J > 0$, in this simple hexagonal lattice leads to spin frustrations. It has been reported that the skyrmion phase is, in principle, possible in frustrated magnets [22,23]. However, such a phase exists only at exceedingly large external fields B comparable to the antiferromagnetic exchange J . That is unusual for most antiferromagnets. In this work, we demonstrate that the scenario of thermally driven topology applies to this antiferromagnetic frustrated spin model as well. Our Monte Carlo simulations reveal that instead of skyrmions, nonzero topological charge takes place at low fields and elevated temperatures. It can thus be easily accessible in experiments. Unlike its ferromagnetic counterpart, in which the skyrmion phase and thermally driven topological phase coexist at low magnetic fields, the thermally driven topological phase is disconnected from

the skyrmion phase in the current antiferromagnetic model. We also proposed a real frustrated system as an example, the Mn-Bi ML film, to enable thermally driven topology in this material.

II. METHODS

A. Monte Carlo simulations

Metropolis Monte Carlo simulations were employed [24] iteratively to generate a Markov chain [25] of spin configurations, which was then used to derive the thermal average of the topological charge by employing the Berg formula in Eq. (1). Periodic boundary conditions were used for 2D hexagonal lattices with a size of 120×120 unless otherwise noted. The local magnetic moment S is normalized so that all the parameters J , D , K_u , and B in the Hamiltonian as well as temperature T have the dimensions of energy and J is set as the units of both energy and temperature. Averages over 2.56×10^6 ensembles are performed at each temperature step during the annealing procedure which starts from $10.0J$, a very high temperature.

B. First-principles calculations

The spin-polarized first-principles calculations using the projector augmented-wave pseudopotential [26,27] implemented in the VASP package [28,29] were performed to calculate electronic and magnetic properties of the Mn-Bi ML films. The local-density approximation (LDA) [30] was employed for the exchange-correlation functional. The wave functions were expanded in plane waves with an energy cutoff of 600 eV throughout the calculations. The k points were sampled on a Γ -centered 15×15 mesh in the 2D Brillouin zone of the unit cell containing one A - B (Mn-Bi) site. Noncollinear magnetic calculations with SOC are included in the total energy calculations for obtaining the magnitude of parameters J , D , and K_u in the Hamiltonian.

III. RESULTS AND DISCUSSION

A. Topological charge driven by thermal fluctuations

As the first model calculation, we choose the parameters in the Hamiltonian with $D = 0.40J$, $K_u = 0.20J$, and $B = 0.40J$. The relation between average topological charge Q_T and temperature is shown in Fig. 2. Topological charge density is zero at very low temperature, while it becomes nonzero at finite temperatures. The dip is located at $T = 0.341J$, with a maximum density of $|Q_T|$ of about 6.07 per 1000 spins. At very high temperatures, Q_T again converges to zero due to the topological triviality of a completely random phase. The same calculations were performed for lattices with sizes ranging from 36×36 to 120×120 . Also we performed one calculation on a 72×72 lattice with open boundary conditions. Almost no difference could be found among them, indicating immunity to the finite-size effect. This robustness of the nonzero topological charge thus originates from the atomic-scale physics.

The dip position of topological charges is close to the phase transition temperature of spin ordering. Specific heat C_v as a function of temperature is shown in Fig. 2. A discontinuous point appears at $T = 0.315J$, indicating a second-order

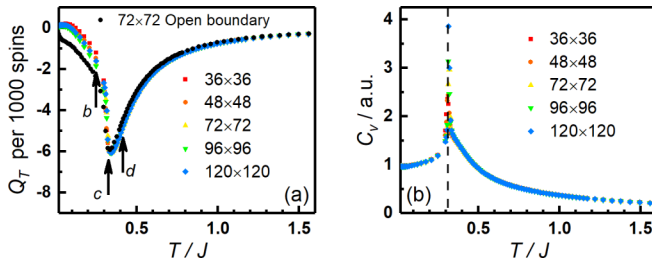


FIG. 2. (a) Topological charge density as a function of temperature in the annealing process with varying lattice sizes. The black one corresponds to the result on a 72×72 lattice with the open boundary condition. (b) Temperature dependence of specific heat on the lattice size. Three arrows labeled *b*, *c*, and *d* indicate the three temperatures $T = 0.249 J$, $0.328 J$, and $0.401 J$, respectively, and the corresponding snapshots are shown in Fig. 3. The dashed line in (b) indicates the phase transition temperature.

phase transition. To further understand the relation between topological charge and the phase transitions, we took snapshots of spin states at $T = 0.020 J$, $0.249 J$, $0.328 J$, and $0.401 J$, as shown in Fig. 3.

The same spin-ordering phases take place at very low temperature $T = 0.02 J$ [Fig. 3(a)] and low temperature $T = 0.249 J$ [Fig. 3(b)], according to both real-space spin textures and corresponding fast Fourier transformation (FFT) images. Three neighbor spins in each triangle belong to three different sublattices in the hexagonal lattice. Spins from each sublattice form a helical state, as shown in Fig. 3(e). Although spin orientations are different, spin helices in these three sublattices have the same spin wave vector \mathbf{q} , so it is called the single- q state [22,23]. As a result, the real-space configuration

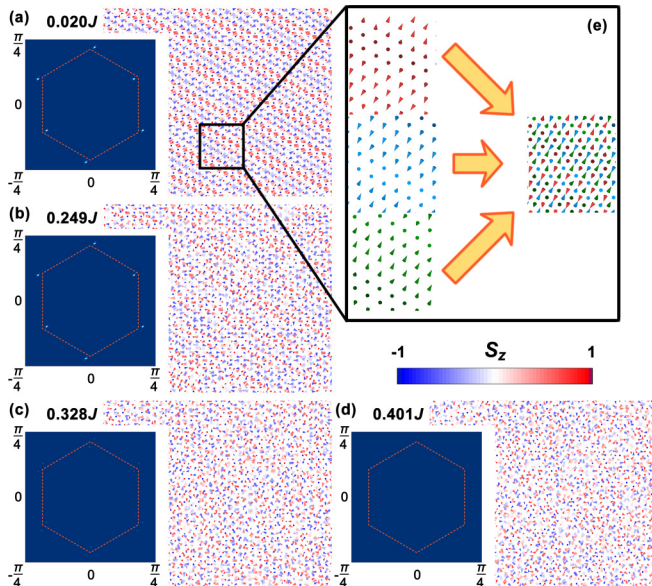


FIG. 3. Snapshots and their corresponding fast Fourier transform (FFT) images at (a) $T = 0.020 J$, (b) $T = 0.249 J$, (c) $T = 0.328 J$, and (d) $T = 0.401 J$, labeled by arrows in Fig. 2(a). The in-plane components of spins are represented by the arrows, while the z component is shown by the color scale. (e) Close-up view of (a) to display the combination of spin helices on three sublattices labeled by different colors.

shows spiral features globally, while in the FFT images, six spots appear in the first Brillouin zone, corresponding to the $\sqrt{3} \times \sqrt{3}$ spin-reconstruction supercell, and the wave vector of each helix corresponds to the offset from each corner of the auxiliary red dashed hexagon in the FFT image. It is obvious that this spin ordering has zero topological charge. It is consistent with previous studies that found that in antiferromagnets [31,32] or frustrated systems [22,23], no skyrmion can be found at low fields.

At $T = 0.328 J$ [Fig. 3(c)], which is just above the phase transition temperature $T_N = 0.315 J$, the spin texture is disordered. No spin-ordered texture can be identified in real space, consistent with the absence of bright spots in the FFT image. But at that temperature, the topological charge density is -5.91 per 1000 spins, a definitely nonzero value. The same situation happens at a higher temperature $T = 0.401 J$ [Fig. 3(d)], which well exceeds the transition temperature. The topological charge density is -5.09 per 1000 spins, while the spin texture is also disordered. Therefore, the above result indicates nontrivial topology bridging over both ordered and disordered states. Although the dip position of topological charge is almost the same as the transition temperature, the appearance of the nonzero topological charge at finite temperature does not have direct correspondence to the phase transition between the ordered helical state and the paramagnetic phase because the topological charge defined in Eq. (1) respects the full rotational symmetry. It cannot be served as an order parameter.

The results above confirm that this frustrated system is another system showing nonzero topological charge at finite temperature, in addition to 2D chiral magnets discussed in our earlier work [13]. Nonzero topological charge in both systems originates from thermally unbalanced local canting and anticanting due to the presence of DM interaction and external magnetic field. Both systems demonstrate similar behaviors in the scaling of Q_T as well. According to the definition in Eq. (1), topological charge Q_T respects the spatial inversion symmetry but breaks the time-reversal symmetry. The inversion symmetry brings about a quadratic relation as the lowest order between Q_T and the DM interaction D , which has odd spatial inversion; the magnetic field B , which has odd time reversal, breaks the time-reversal symmetry, so that Q_T is proportional to B . As a result, the magnitude of topological charge must scale as

$$Q_T \propto D^2 B. \quad (3)$$

The same argument applies to the current system, and a similar relation holds. Figures 4(a) and 4(c) show the D dependence of the topological charge density. Annealing curves show that the dip positions of topological charge density are almost unchanged, while the dip values increase as D increases. As shown in Fig. 4(c), the value of the topological charge density $|Q_T|$ has a quadratic dependence on D at $T = 1.49 J$. This quadratic relation is also robust all the way to high temperatures. On the other hand, the relation between the topological charge density and B is shown in Figs. 4(b) and 4(d). An upward trend in $|Q_T|$ with increasing B is quite similar to that of the $|Q_T| - D$ relation in Fig. 4(b). A detailed investigation shows that $|Q_T|$ is proportional to B [Fig. 4(d)].

Although the nontrivial topology in this antiferromagnetic frustrated system has exactly the same relation with D and B

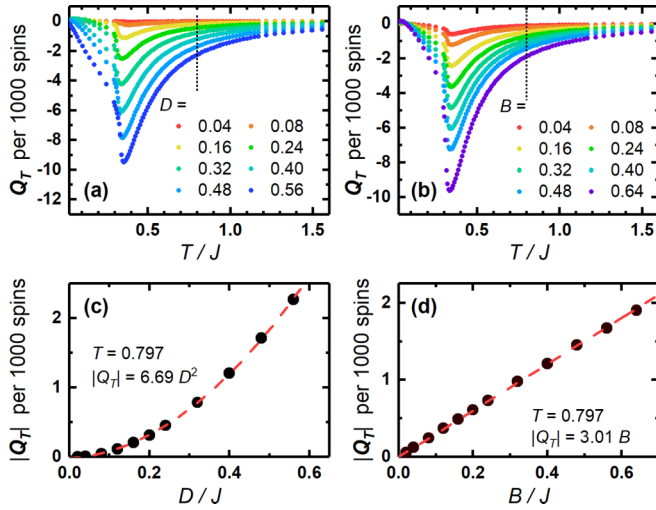


FIG. 4. Dependence of the topological charge on the DM interaction and external magnetic field. Topological charge density as a function of temperature with varying (a) D and (b) B . In (a), $B = 0.4J$ and $K_u = 0.2J$ are fixed, and in (b), $D = 0.4J$ and $K_u = 0.2J$ are fixed. Values of topological charge density $|Q_T|$ as a function of (c) D and (d) B at $T = 0.797J$ are shown by the dotted lines in (a) and (b).

as that in ferromagnetic chiral magnets at high temperatures, a significant difference, however, appears at low temperatures. In chiral magnets, skyrmions appear at low temperatures when the field is appropriate and contribute to the topological charge density in addition to the thermal fluctuation. Thermally driven topology coexists with skyrmions [13]. But in the current frustrated system, the single- q state, a topologically trivial state, prevails below the transition temperature. The only source of topological charge is the thermal fluctuation. It is thus a system in which topology is purely thermally driven.

The uniaxial magnetic anisotropy K_u dependence of the topological charge was also investigated. The results are shown in Fig. 5(a). Other parameters were fixed to $D = 0.40J$ and $B = 0.40J$. As shown in Fig. 5(a), the dip positions of the topological charge increase as K_u grows, but the dip values decrease. According to Fig. 5(c) with two magnetic field values $B = 0.10J$ and $0.40J$, the value of the topological charge $|Q_T|$ has a linear relation with K_u at high temperatures. This still obeys the symmetry principle since K_u respects both the inversion symmetry and the time-reversal symmetry. According to the linear fitting under two different magnetic fields, it can be written as $|Q_T| \propto B(K_u + 1.70)$ or $|Q_T| \propto B(1 + \alpha K_u)$, with $\alpha = 0.59 J^{-1}$. As a result, based on Eq. (3), the thermally driven topological charge in this system has the relation

$$Q_T \propto D^2 B(1 + \alpha K_u), \quad \alpha > 0, \quad (4)$$

at high temperatures.

K_u has a behavior similar to external magnetic field at high temperatures since K_u can be regarded as an effective magnetic field $B_{\text{eff},i}^{(K_u)} = K_u S_{iz}$. Since this effective field is just an additional magnetic field, the intercept in Fig. 5(c) is nonzero when $B \neq 0$. On the other hand, the dip positions of topological charges increase because the phase transition

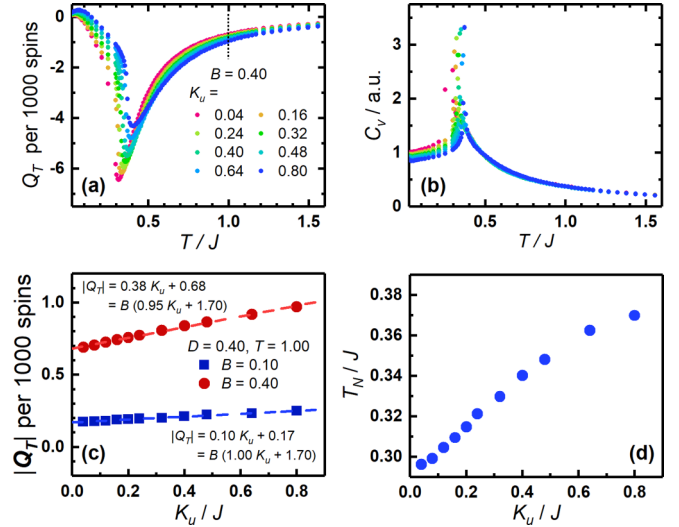


FIG. 5. Relationship between topological charge and uniaxial magnetic anisotropy. (a) Topological charge density and (b) specific heat as functions of temperature under varying values of K_u with $D = 0.40J$ and $B = 0.40J$. (c) The value of topological charge density as a function of K_u at $T = 1.00J$ [dotted line in (a)] with two magnetic field values, $B = 0.10J$ and $0.40J$. (d) Phase transition temperature T_N as a function of K_u .

temperature is enlarged by K_u . The K_u dependence of specific heat C_V as a function of temperature is shown in Fig. 5(b). The discontinuous point of C_V moves to the right as K_u increases, indicating the increasing of the phase transition temperature. Figure 5(d) shows the relation between the phase transition temperature T_N and K_u . $T_N = 0.29J$ without magnetic anisotropy and increases about 27% when K_u reaches $0.80J$.

B. Mn-Bi thin film from first-principles calculations

This 2D frustrated model is a prototype of many non-centrosymmetric magnetic thin-film systems. Particularly, it is the lattice of Mn-Bi ML films, where Mn atoms occupy the A sites and Bi atoms sit on B sites. The hexagonal NiAs phase of MnBi is ferromagnetic with a high Curie temperature over 600 K due to large magnetization and strong exchange interaction. It has high coercivity with a rectangular hysteresis loop due to large room-temperature perpendicular anisotropy [33–37]. Although there is no DM interaction in bulk MnBi as the inversion symmetry is respected, the inversion symmetry can be easily broken in the ML films.

To construct Mn-Bi thin films, we chose a graphene sheet as the substrate to stabilize the structure. This is because graphene can build good interfaces with many metal thin films [38–41]. Also, the in-plane lattice constant of MnBi bulk of 4.28 \AA is quite close to that of $\sqrt{3} \times \sqrt{3}$ graphene lattice of 4.26 \AA . According to the LDA functional calculations, the in-plane lattice constant is relaxed to 4.24 \AA in one unit cell (uc) and still matches the experimental results. Two MLs of Mn and one ML of Bi are placed on the graphene sheet. The most stable structure with lowest total energy is shown in Fig. 6(a). Two Mn MLs are located between graphene and the Bi ML, and the lower Mn layer is located on the hexagonal hollow of graphene with a Mn-C bond length of 2.11 \AA , indicating the

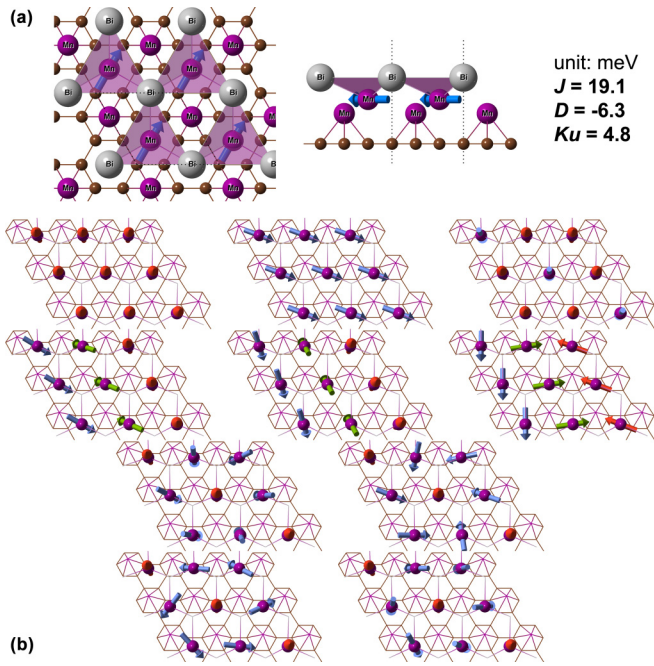


FIG. 6. (a) Top and side views of the structure of 2 ML of Mn (violet balls) and 1 ML of Bi (gray balls) on a graphene substrate (brown balls). (b) Ten spin configurations used to perform total energy calculations for obtaining J , D , and K_u . The final results are also displayed.

robustness of the interface. According to the self-consistent calculations, the lower Mn layer has no magnetization, while the local magnetic moment of the upper Mn ML is $3.2 \mu_B$.

To get the magnitude of the parameters J , D , and K_u , we set ten noncollinear spin configurations on the upper ML Mn atoms, shown in Fig. 6(b), and calculated the total energies for each of them. A set of super rank equations based on the Hamiltonian in Eq. (2) was built, and all the parameters can be obtained. The results are $J = 19.1$ meV/uc, $D = -6.3$ meV/uc, and $K_u = 4.8$ meV/uc, also shown in Fig. 6(a). Here J is positive, indicating the antiferromagnetic coupling that was expected. Due to the hexagonal lattice, this Mn-Bi thin-film system is truly a spin-frustrated system. K_u is also positive, so it has uniaxial magnetic anisotropy. D is nonzero and negative due to the presence of Bi atoms right on top of the Mn ML, resulting in the clockwise direction DM interaction around one magnetic moment.

A remarkable observation here is that the magnitude of D is quite large. This lattice model value of D can also be converted into the continuum model using $\tilde{D} = D(a/\Omega)$, where a is the in-plane lattice constant and Ω is the volume of the unit cell. Therefore, we have $\tilde{D} = -7.0$ mJ/m², about four times larger than that in the chiral magnet FeGe [42]. The ratio of D and J is about 1/3, close to the parameters $D = 0.4J$ in the Monte Carlo simulations above.

C. Topology in the Mn-Bi thin film

As all necessary parameters in Eq. (2) have been obtained in the Mn-Bi thin film, we redid the Monte Carlo simulations to study both the spin ordering and topology in this real

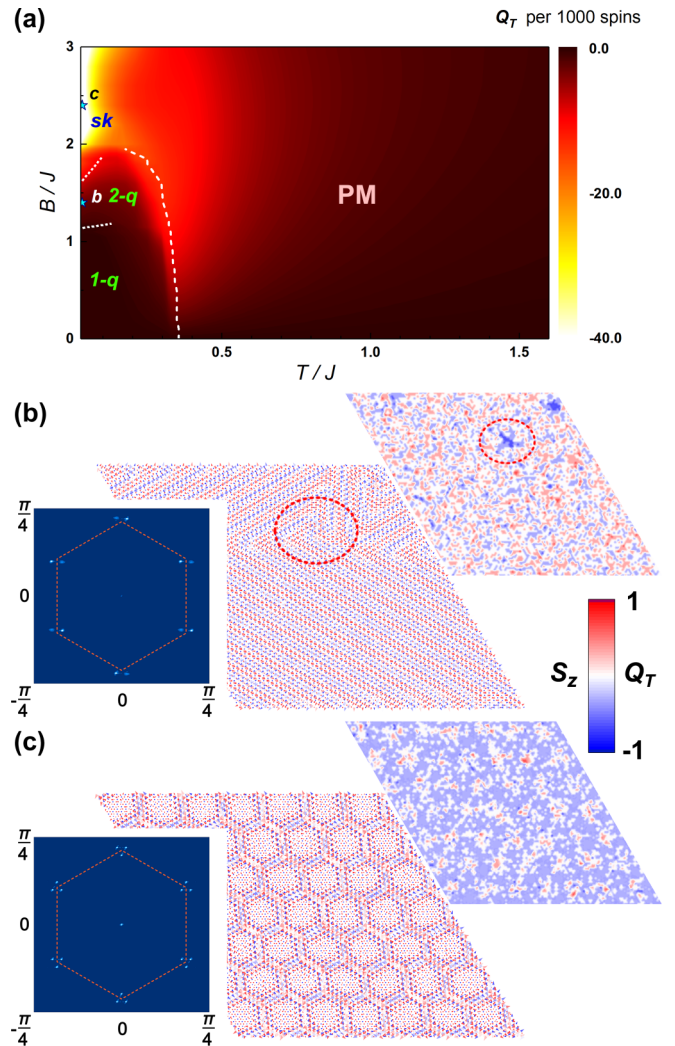


FIG. 7. In the Mn-Bi thin-film system, (a) the phase diagram of topological charge densities with the magnetic field and temperature dependence. The dip positions are connected by a dashed line. Two white dotted lines divide the region of single- q ($1-q$), double- q ($2-q$), and skyrmion (sk) states, respectively. Stars labeled b and c correspond to the snapshots in (b) and (c). Snapshots of spin textures and the corresponding FFT images and distribution of topological charge density with (b) $B = 1.4J$ and (c) $B = 2.4J$ at very low temperature $T = 0.02J$. The color bar gives the color map of the z component of spins and the value of topological charge density.

system. Figure 7(a) gives the B - T diagram of topological charge density as a function of the magnetic field B and temperature T . At low magnetic fields, topological charge density is zero at both very low and very high temperatures, but there is a ridge showing nonzero values near the phase transition temperature. At high temperatures, $|Q_T|$ increases as B increases. Therefore, it is consistent with the numerical simulations above, indicating that the thermally driven topology dominates at the low-field region in the Mn-Bi thin film.

When $B > 1.1J$, the value of topological charge becomes nonzero at low temperatures. According to the snapshot taken at $B = 1.4J$, as shown in Fig. 7(b), two helical stripes appear in the real space and form a double- q state. The two helices

form an angle of 120° with respect to each other, resulting in two bright spots near each corner of the auxiliary hexagon in the reciprocal space. Although the distribution of topological charge density looks pretty random in the whole lattice, the intersections between two helices demonstrate considerably large local topological charge density, as shown in the dashed circles in Fig. 7(b).

As the magnetic field continues to increase, the number of topological charges grows as well, especially at low temperatures. Around $B = 1.8J$, however, another phase transition takes place. The number of topological charges increases swiftly and has a dip value of over -58 per 1000 atoms at $B = 2.2J$. The snapshot at $B = 2.4J$ gives a honeycomblike lattice of spin texture, as shown in Fig. 7(c). In the reciprocal space, three spots appear near each corner of the auxiliary hexagon so that each sublattice has three helices, whose wave vectors expand an angle of 120° with respect to each other. The combination of three spin helices is nothing but the skyrmion crystal lattice, so that each sublattice forms one skyrmion lattice. The total spin texture is the combination of these three skyrmion lattices, and the centers of skyrmions form a hexagonal lattice.

In skyrmion lattices found in ferromagnetic chiral magnets, each skyrmion gives -1 topological charge. Since only 50 skyrmions in the 96×96 lattice, where there should be about -5 topological charges per 1000 spins, are identified according to the spin texture in Fig. 7(c), this number is far from the total value of the topological charge we counted, which is -55 . This discrepancy occurs because three neighboring spins on each triangle belong to different sublattices. Because of the antiferromagnetic coupling, a large solid angle is formed among the neighboring spins, leading to the large local density of topological charge, so that the density of topological charge, shown in 7(c), gives an almost uniform density in the whole lattice, incommensurate with the overarching skyrmion lattice. Therefore, the skyrmion phase in this frustrated system has distinct nontrivial topology with the skyrmion phase in ferromagnets. Both double- q and skyrmion crystal phases at low temperatures consist with previous studies on frustrated systems [22,23].

One should note that the critical magnetic field for the skyrmion phase is about $B = 2.0J$. Since $J \sim 20$ meV and magnetic momentum $m_s = 3.2\mu_B \sim 0.19$ meV/T in the Mn-Bi thin film, the critical field is about 200 T, which cannot be reached experimentally. Even the double- q state requires a field of $B = 1.1J \sim 100$ T. As a result, under a very wide range of experimentally accessible fields, thermally driven topology is the only source of nontrivial topology in this system.

IV. SUMMARY

In conclusion, we have studied the topological properties in an antiferromagnetic frustrated hexagonal lattice. In a very wide range of magnetic fields, thermally driven topology is the only nontrivial topology at finite temperatures. The magnitude of topological charge has the relation $Q_T \sim D^2B(1 + \alpha K_u)$ with respect to the DM interaction D , magnetic field B , and uniaxial magnetic anisotropy K_u in the high-temperature region. The Mn-Bi thin-film system on a graphene sheet is a proposed real system to enable this phenomenon. The magnitudes of J , D , and K_u used for model calculations based on Eq. (2) are identified via first-principles calculations. Although both double- q and skyrmion states are found at very high magnetic fields, thermally driven topology is the only source of topological charge under reasonable fields. But we have to emphasize that Mn-Bi thin films will not be the only example. The thermally driven topology in an antiferromagnetic system is far more general. More materials and experiments, such as the magnon Hall effects, are expected.

ACKNOWLEDGMENTS

This work was supported by the U.S. Department of Energy (DOE), Office of Science, Basic Energy Sciences (BES) under Award No. DE-SC0016424. First-principles calculations used the Extreme Science and Engineering Discovery Environment (XSEDE) under Grant No. TG-PHY170023 and Monte Carlo simulations were performed on Trillian, a Cray XE6m-200 supercomputer at UNH supported by the NSF MRI program under Grant No. PHY-1229408.

-
- [1] S. Muhlbauer, B. Binz, F. Jonietz, C. Pfleiderer, A. Rosch, A. Neubauer, R. Georgii, and P. Boni, *Science* **323**, 915 (2009).
 - [2] A. Neubauer, C. Pfleiderer, B. Binz, A. Rosch, R. Ritz, P. G. Niklowitz, and P. Böni, *Phys. Rev. Lett.* **102**, 186602 (2009).
 - [3] A. Bogdanov and A. Hubert, *J. Magn. Magn. Mater.* **138**, 255 (1994).
 - [4] X. Z. Yu, N. Kanazawa, Y. Onose, K. Kimoto, W. Z. Zhang, S. Ishiwata, Y. Matsui, and Y. Tokura, *Nat. Mater.* **10**, 106 (2011).
 - [5] W. Jiang, X. Zhang, G. Yu, W. Zhang, X. Wang, M. B. Jungfleisch, J. E. Pearson, X. Cheng, O. Heinonen, K. L. Wang *et al.*, *Nat. Phys.* **13**, 162 (2016).
 - [6] W. Jiang, G. Chen, K. Liu, J. Zang, S. G. te Velthuis, and A. Hoffmann, *Phys. Rep.* **704**, 1 (2017).
 - [7] X. Z. Yu, Y. Onose, N. Kanazawa, J. H. Park, J. H. Han, Y. Matsui, N. Nagaosa, and Y. Tokura, *Nature (London)* **465**, 901 (2010).
 - [8] B. Berg and M. Lüscher, *Nucl. Phys. B* **190**, 412 (1981).
 - [9] N. Nagaosa and Y. Tokura, *Nat. Nanotechnol.* **8**, 899 (2013).
 - [10] G. Yin, Y. Li, L. Kong, R. K. Lake, C. L. Chien, and J. Zang, *Phys. Rev. B* **93**, 174403 (2016).
 - [11] I. Dzyaloshinsky, *J. Phys. Chem. Solids* **4**, 241 (1958).
 - [12] T. Moriya, *Phys. Rev.* **120**, 91 (1960).
 - [13] W.-T. Hou, J.-X. Yu, M. Daly, and J. Zang, *Phys. Rev. B* **96**, 140403 (2017).
 - [14] S. X. Huang and C. L. Chien, *Phys. Rev. Lett.* **108**, 267201 (2012).
 - [15] M. Mochizuki, X. Z. Yu, S. Seki, N. Kanazawa, W. Koshibae, J. Zang, M. Mostovoy, Y. Tokura, and N. Nagaosa, *Nat. Mater.* **13**, 241 (2014).
 - [16] J. Iwasaki, A. J. Beekman, and N. Nagaosa, *Phys. Rev. B* **89**, 064412 (2014).

- [17] M. Hirschberger, R. Chisnell, Y. S. Lee, and N. P. Ong, *Phys. Rev. Lett.* **115**, 106603 (2015).
- [18] H. Lee, J. H. Han, and P. A. Lee, *Phys. Rev. B* **91**, 125413 (2015).
- [19] S. Heinze, K. von Bergmann, M. Menzel, J. Brede, A. Kubetzka, R. Wiesendanger, G. Bihlmayer, and S. Blügel, *Nat. Phys.* **7**, 713 (2011).
- [20] J. Grenz, A. Köhler, A. Schwarz, and R. Wiesendanger, *Phys. Rev. Lett.* **119**, 047205 (2017).
- [21] A. Palacio-Morales, A. Kubetzka, K. von Bergmann, and R. Wiesendanger, *Nano Lett.* **16**, 6252 (2016).
- [22] T. Okubo, S. Chung, and H. Kawamura, *Phys. Rev. Lett.* **108**, 017206 (2012).
- [23] A. O. Leonov and M. Mostovoy, *Nat. Commun.* **6**, 8275 (2015).
- [24] N. Metropolis and S. Ulam, *J. Am. Stat. Assoc.* **44**, 335 (1949).
- [25] S. Buhrandt and L. Fritz, *Phys. Rev. B* **88**, 195137 (2013).
- [26] P. E. Blöchl, *Phys. Rev. B* **50**, 17953 (1994).
- [27] G. Kresse and D. Joubert, *Phys. Rev. B* **59**, 1758 (1999).
- [28] G. Kresse and J. Furthmüller, *Comput. Mater. Sci.* **6**, 15 (1996).
- [29] G. Kresse and J. Furthmüller, *Phys. Rev. B* **54**, 11169 (1996).
- [30] J. P. Perdew and A. Zunger, *Phys. Rev. B* **23**, 5048 (1981).
- [31] X. Zhang, Y. Zhou, and M. Ezawa, *Sci. Rep.* **6**, 24795 (2016).
- [32] B. Göbel, A. Mook, J. Henk, and I. Mertig, *Phys. Rev. B* **96**, 060406 (2017).
- [33] K. Egashira and T. Yamada, *J. Appl. Phys.* **45**, 3643 (1974).
- [34] X. Guo, X. Chen, Z. Altounian, and J. O. Ström-Olsen, *Phys. Rev. B* **46**, 14578 (1992).
- [35] G. Di, S. Iwata, S. Tsunashima, and S. Uchiyama, *J. Magn. Magn. Mater.* **104-107**, 1023 (1992).
- [36] P. M. Oppeneer, V. N. Antonov, T. Kraft, H. Eschrig, A. N. Yaresko, and A. Y. Perlov, *J. Appl. Phys.* **80**, 1099 (1996).
- [37] J. B. Yang, K. Kamaraju, W. B. Yelon, W. J. James, Q. Cai, and A. Bollero, *Appl. Phys. Lett.* **79**, 1846 (2001).
- [38] Y. Kim, J. Lee, M. S. Yeom, J. W. Shin, H. Kim, Y. Cui, J. W. Kysar, J. Hone, Y. Jung, S. Jeon *et al.*, *Nat. Commun.* **4**, 2114 (2013).
- [39] Y. Jiang, Y. Y. Sun, M. Chen, Y. Wang, Z. Li, C. Song, K. He, L. Wang, X. Chen, Q.-K. Xue *et al.*, *Phys. Rev. Lett.* **108**, 066809 (2012).
- [40] Q. Ran, M. Gao, X. Guan, Y. Wang, and Z. Yu, *Appl. Phys. Lett.* **94**, 103511 (2009).
- [41] C. Gong, G. Lee, B. Shan, E. M. Vogel, R. M. Wallace, and K. Cho, *J. Appl. Phys.* **108**, 123711 (2010).
- [42] T. Koretsune, N. Nagaosa, and R. Arita, *Sci. Rep.* **5**, 13302 (2015).